J. Fluid Mech. (2003), *vol.* 475, *pp.* 147–162. © 2003 Cambridge University Press
DOI: 10.1017/S0022112002002732 Printed in the United Kingdom

Amplitude growth rate of a Richtmyer–Meshkov unstable two-dimensional interface to intermediate times

By NORMAN J. ZABUSKY, ALEXEI D. KOTELNIKOV, YURIY GULAK AND GAOZHU PENG
Department of Mechanical and Aerospace Engineering and CAIP Center, Rutgers University,
98 Brett Road, Piscataway, NJ 08854, USA

(Received 19 January 2000 and in revised form 5 August 2002)

The Richtmyer–Meshkov instability in an incompressible and compressible stratified two-dimensional ideal flow is studied analytically and numerically. For the incompressible problem, we initialize a single small-amplitude sinusoidal perturbation of wavelength λ, we compute a series expansion for the amplitude a in powers of t up to $t^{(11)}$ with the MuPAD computer algebra environment. This involves harmonics up to eleven. The simulations are performed with two codes: incompressible, a vortex-in-cell numerical technique which tracks a single discontinuous density interface; and compressible, PPM for a shock-accelerated case with a finite interfacial transition layer (ITL). We identify properties of the interface at time $t = t_M$ at which it first becomes 'multivalued'. Here, we find the normalized width of the 'spike' is related to the Atwood number by $(w_m/\lambda) - 0.5 = -0.33A$. A high-order Padé approximation is applied to the analytical series during early time and gives excellent results for the interface growth rate $\dot{a}$. However, at intermediate times, $t > t_M$, the agreement between numerical results and different-order Padé approximants depends on the Atwood number. During this phase, our numerical solutions give $\dot{a} \propto O(t^{-1})$ for small A and $\dot{a} \propto O(t^{-0.4})$ for $A = 0.9$. Experimental data of Prasad *et al.* (2000) for SF_6 (post shock Atwood number = 0.74) shows an exponent between -0.68 and -0.72 and we obtain -0.683 for the compressible simulation. For this case, we illustrate the important growth of vortex-accelerated (secondary) circulation deposition of both signs of vorticity and the complex nature of the roll-up region.

1. Introduction

A perturbed interface between two fluids of different densities acquires vorticity if it is subjected to an impulsive acceleration, for example, as caused by a shock wave or by time-dependent gravity effects. The baroclinically deposited primary vorticity on the interface drives the interface evolution, a phenomenon called the Richtmyer–Meshkov (RM) instability. The RM instability is of crucial importance for research in supernova astrophysics, inertial confinement fusion (ICF) and supersonic combustion. It has been studied over many years: analytically (e.g. Layzer 1955; Haan 1991; Hecht, Alon & Shvarts 1994; Samtaney & Pullin 1996); numerically (e.g. Meyer & Blewett 1972; Youngs 1984; Picone & Boris 1988; Tryggvason 1988; Hawley & Zabusky 1989; Mikaelian 1993; Grove 1994); and experimentally (e.g. Meshkov 1969; Andronov *et al.* 1976; Zaytsev *et al.* 1985; Dimonte & Remington 1993; Jacobs *et al.* 1995; Aleshin *et al.* 1997). A review of this work which emphasizes the vortex paradigm was given by Zabusky (1999).

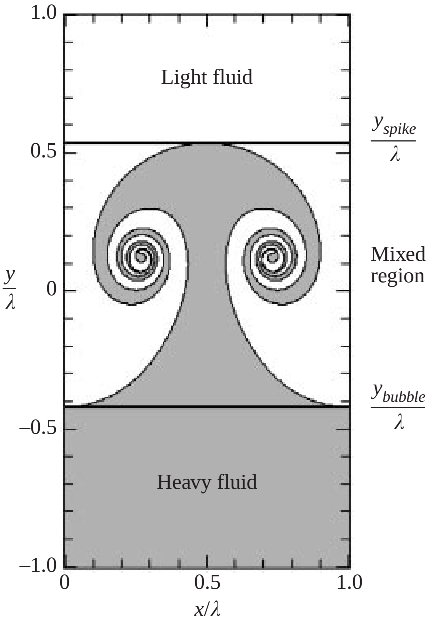

FIGURE 1. Schematic of the waveform of the evolved interface for a Richtmyer–Meshkov instability.

For our analysis and simulations, we examine the classical configuration – a planar interface orthogonal to the exciting gravity with a very small-amplitude sinusoidal perturbation. Based on previous shock–interface studies (Zabusky 1999) and one new run in this paper, we assume that there is a circulation per unit length on this interface which has an identical single harmonic distribution to the amplitude. This gives rise to a velocity jump tangential to the interface of $2v_0$. The evolution proceeds through several phases: 'very early time', where a linear analysis suffices; 'early time', where nonlinear effects are important; 'intermediate time', where the interface undergoes multiple rolls producing the well-known 'mushroom' configuration, as shown in figure 1; and late time. The time between early and intermediate we take as the time when the interface first becomes multivalued, or $t = t_M$, as already introduced in Zabusky (1999). Note, if we had perturbed the interface with an additional very small-wavelength perturbation of very small amplitude, it would have become multivalued much earlier. We assume that these very small wavelengths are not present initially.

The parameters which define the problem are the density ratio or Atwood number $A = (\rho_2 - \rho_1)/(\rho_2 + \rho_1)$, the normalized perturbation amplitude, $a_0/\lambda = ka_0/2\pi$, and v_0, which is related to the circulation on the interface. A simple quantifier of the interface evolution is the 'growth rate' of the interfacial amplitude, defined as the time rate of change of half the distance between the 'spike' and the 'bubble', the highest and lowest points, respectively, of the interface in figure 1. Note that the natural variable to normalize time is λ/v_0.

The compressible linear phase was studied first by Richtmyer (1960) who derived a linear 'impulsive model' for the growth rate. Yang, Zhang & Sharp (1994) made a detailed study of the linear phase and validated the parameter ranges where the Richtmyer model was useful. If the approaching shock is weak, the flow behind the shock rapidly becomes nearly incompressible as the shock moves away from the weakly perturbed interface, as discussed by Pham & Meiron (1993), Meiron & Meloon (1997) and Kotelnikov, Ray & Zabusky (2000). Wouchuk & Nishihara (1996,

1997) also discussed the physical effects of strong shocks and the reduction of the growth rate which results from the vorticity deposited in the bulk by the curved transmitted shock.

For an incompressible regime, attempts were made to calculate analytically non-linear estimates for the growth rate based on a few term Taylor series expansion by Haan (1991) and Zhang & Sohn (1996). However, no analysis exists which treats the 'multivalue' time and beyond.

The work presented below presents a longer time carefully juxtaposed analytical and numerical study. In § 2, we describe analytical and numerical techniques for calculating interface evolution and present numerical results. In particular, we discuss the time and shape of the interface and its circulation for different Atwood numbers at the multivalued time. In § 3, we compare the Padé approximant resummation of the analytical Taylor series with the numerical results. In § 4, we discuss caveats for calculating beyond intermediate times because of the manifestations of a singularity on the interface when computing with Euler codes.

2. Analytical and numerical solutions for the evolution of the RM instability with a sinusoidal interface

2.1. *Power series solution in the small amplitude/wavelength ratio a_0/λ*

In this section, we extend the analytical technique proposed by Zhang & Sohn (1996) to higher order and discuss the limitations of their suggested arbitrary Padé approach.

We consider a single-valued two-dimensional interfacial curve $y = \eta(x, t)$ separating two ideal incompressible fluids of different densities ρ_1 and ρ_2. Initially, at $t = 0$, the interface has a sinusoidal form of wavelength λ $(= 2\pi/k)$ and amplitude a_0

$$\eta(x, 0) = a_0 \cos(kx). \tag{1}$$

We assume that the flow velocities $\boldsymbol{v}_i$ off the interface, are irrotational and can be obtained from velocity potentials

$$\boldsymbol{v}_i = -\nabla\varphi_i \quad \text{for } i = 1, 2. \tag{2}$$

where the velocity potential in each fluid satisfies the Laplace equation:

$$\nabla^2\varphi_i(x, y, t) = 0 \quad \text{for } i = 1, 2. \tag{3}$$

The initial conditions for φ_1 and φ_2 are assumed to have the same harmonic dependence as the interface

$$\varphi_1 = (v_0/k)\, \mathrm{e}^{-ky} \cos(kx), \quad \varphi_2 = (-v_0/k)\, \mathrm{e}^{+ky} \cos(kx). \tag{4}$$

Such a phenomenon would occur if a weak shock were to hit a small-amplitude sinusoidally perturbed density interface, as described by Kotelnikov *et al.* (2000 § 111). Note that kv_0 is the initial linear rate of change of the interface and is related to the circulation deposited on the interface by the weak shock wave. The use of an interfacial curve (rather than a thin layer) makes this an ill-posed problem, as discussed by Baker, Caflisch & Siegel (1993). This is manifest in the uncontrolled small-scale structure which appears at a fixed time as the resolution increases, which we observe and discuss in § 5.

To match the two potentials φ_1 and φ_2, we use two boundary conditions:

(i) kinematic, normal velocity continuity (or $D_t\ (y - \eta) = 0$)

$$\partial_t\eta - \partial_x\varphi_i\partial_x\eta + \partial_y\varphi_i = 0 \quad \text{at } y = \eta \quad \text{for } i = 1 \text{ and } 2. \tag{5}$$

(ii) dynamic, pressure continuity

$$-\rho_1\partial_t\varphi_1+\rho_2\partial_t\varphi_2-\tfrac{1}{2}\rho_2[(\partial_x\varphi_2)^2+(\partial_y\varphi_2)^2]+\tfrac{1}{2}\rho_1[(\partial_x\varphi_1)^2+(\partial_y\varphi_2)^2]=0 \quad \text{at } y=\eta, \tag{6}$$

as obtained from Bernoulli's equation.

Following the procedure of Zhang & Sohn, we assume that the single exponential z-dependence of the potentials persists and the harmonic x-dependence of density and potentials persists to higher modes via nonlinear mode coupling or

$$\left.\begin{aligned}
\eta &= \sum_{p=1}^{\infty}\eta^{(p)}(x,t) && \text{where } \eta^{(p)} = \sum_{j=1}^{j=p}\eta_j^{(p)}(t)\cos(jx),\\
\varphi_1 &= \sum_{p=1}^{\infty}\varphi_1^{(p)}(x,y,t) && \text{where } \varphi_1^{(p)} = \sum_{j=1}^{j=p}\phi_{1,j}^{(p)}(t)\mathrm{e}^{-jky}\cos(jx),\\
\varphi_2 &= \sum_{p=1}^{\infty}\varphi_2^{(p)}(x,y,t) && \text{where } \varphi_2^{(p)} = \sum_{j=1}^{j=p}\phi_{2,j}^{(p)}(t)\mathrm{e}^{+jky}\cos(jx).
\end{aligned}\right\} \tag{7}$$

However, we use the MuPAD (1996) computer algebra environment to perform the lengthy algebraic calculations and thereby generate a nine-term literal series. MuPAD expands $\eta_j^{(p)}, \varphi_{1,j}^{(p)}$ and $\varphi_{2,j}^{(p)}$ in integer powers of a_0k and substitutes into the boundary continuity conditions (5) and (6). Then, it sets $y=\eta(x,t)$ and uses the orthogonality relations of $\cos(jx)$ to gather like terms. The Appendix presents the normalized $\eta^{(p)}$, for $p=1$ to $p=6$, and those for $p=7$ to 9 are available from the authors or the *Journal of Fluid Mechanics* Editorial Office, Cambridge. The restriction to nine terms was governed by our computer memory of 2 Gigabytes. However, with specific numerical values for the parameters, we were able to obtain eleven series terms and these representations are used below when comparing with numerical solutions of $\dot{a}$.

$$\dot{a} \equiv \tfrac{1}{2}(v_{spike}-v_{bubble}) = \tfrac{1}{2}(\partial_t\eta(\lambda/2,t)-(\partial_t\eta(0,t)) \tag{8}$$

However, this series would not represent the solution after the singularity arises. Also, practically speaking, the series diverges quickly and rational fraction Padé resummation techniques have been used to regularize this divergence by Zhang & Sohn (1996). We will see how Padé resummation techniques that employ our higher-order series are arbitrary, and the prescription of Zhang & Sohn seems accidental.

However, we sufficiently improved the convergence of the series by performing the re-summation technique differently from Zhang & Sohn (1996): at first, the Padé approximant of $y=\eta(x,t)$ was computed and then its time derivative was obtained. This order of calculations improves the convergence of the series.

2.2. *Numerical results for the interface evolution: incompressible*

We now present results from the incompressible time-dependent numerical method which combines the semi-Lagrangian contour advection and adaptive node redistribution algorithm of Dritschel & Ambaum (1997) with the vortex-in-cell (VIC) method of Tryggvason (1988). This allows us to compute beyond the time when the interface is single-valued. The algorithm is described in Appendix A of Kotelnikov *et al.* (2000). Essentially, there are three processes per step: (i) advect the interfacial contour using velocities at each node and readjust the spacing between the nodes so that their density is related to the curvature of the interface; (ii) solve the ODE for the interfacial circulation γ_s; (iii) project the interfacial circulation onto a uniform doubly periodic mesh to obtain vorticity and use FFT to solve Poisson's equation for

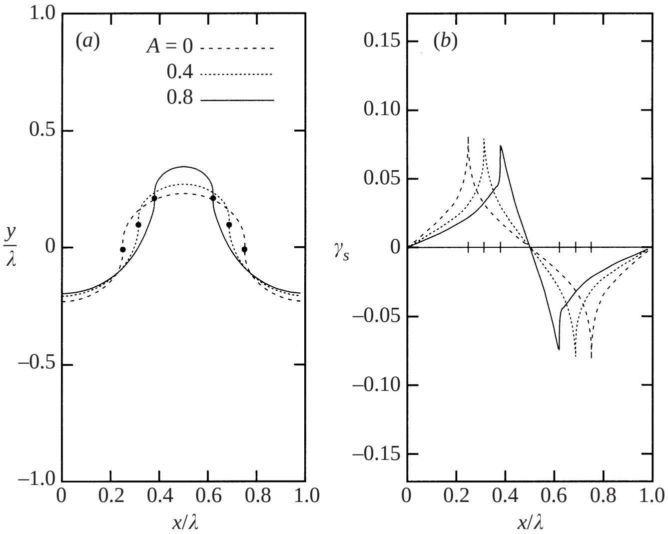

FIGURE 2. (*a*) Interface for three different Atwood numbers at the normalized 'multivalue' time $t_M \sim 6$. (*b*) Circulation per unit length γ_s for three different Atwood numbers at 'multivalue' time $t_M \sim 6$. Parameters are $a_0/\lambda = 0.05$, $v_0/\lambda = 0.04$. The appropriate normalization time is $t_N = a_0/v_0 = 1.25$.

the stream function and velocities at each mesh point. Interpolate the velocities back to the contour nodes. Note, the circulation per unit length at the interface can be expressed in terms of the derivatives of the velocity potential at the interface

$$\gamma_s \equiv (\boldsymbol{v}_1 - \boldsymbol{v}_2)\cdot \boldsymbol{s} = [\partial_x\phi_1 - \partial_x\phi_2 + \partial_x\eta(\partial_y\phi_1 - (\partial_y\phi_2))]|_s/[1 + (\partial_x\eta)^2]^{1/2}, \tag{9}$$

where $\boldsymbol{s}$ is a unit vector tangential to the interface. The initial conditions are as given in (1) and (4) and determine the initial circulation on the interface. We normalize the amplitude and growth rate by the wavelength $\lambda = 2\pi$ or $k = 1.0$. All runs were carried out on a doubly periodic domain of 64×128, namely λ was discretized with 64 intervals, as shown in figure 1. Here we see the y-extrema of the interface designated as 'spike' and 'bubble'.

First, we present simulations for a small-amplitude case, $a_0/\lambda = 0.05$, $v_0/\lambda = 0.04$. The appropriate normalization time is $t_N = a_0/v_0 = 1.25$. The periodicity in y does not affect the comparison below to the algebraic results for the infinite y domain as the interface is far from the boundaries. Below, we discuss the effect of higher resolution and ill-posedness.

Figure 2 shows the interface for three different A at the 'multivalue' time, t_M i.e. where the interface becomes a multivalued function of x. This time is about six for all incompressible runs and the spike-to-bubble amplitude has grown by a factor of five. Figure 2(*b*) shows γ_s *vs.* x and we see that the larger A, the closer is the extremum to the spike point. Note, these extrema correspond to the filled circles in figure 2(*b*) and this is the location where the singularity will develop as we refine the mesh. $A = 0$ corresponds to the Kelvin–Helmholtz instability and the positive circulation per unit length is symmetrical about $\lambda/s = 0.25$, etc. The approach of the extrema to the spike is a manifestation of baroclinic effects. That is, the larger A, the larger the net circulation closer to the spike. Figure 3 shows the width of the finger (distance between the filled circles) normalized by the wavelength, W_m/λ. This linear variation

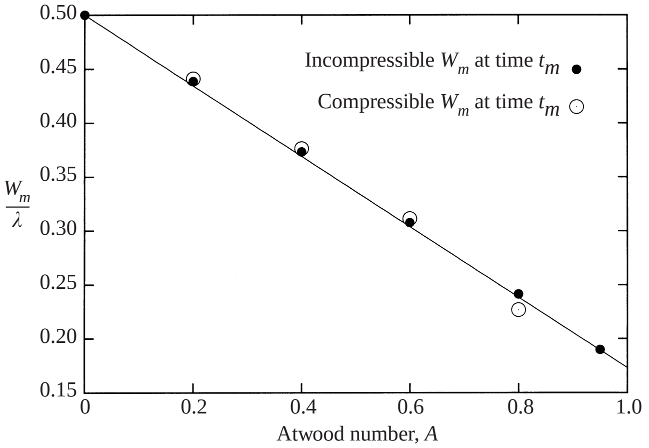

FIGURE 3. Scaling of the 'spike thickness' W_m with Atwood number, at 'multivalue' time $t_M \sim 6$, in the incompressible and compressible numerical simulations. Parameters are $a_0/\lambda = 0.05$, $v_0/\lambda = 0.04$. The appropriate normalization time is $t_N = a_0/v_0 = 1.25$.

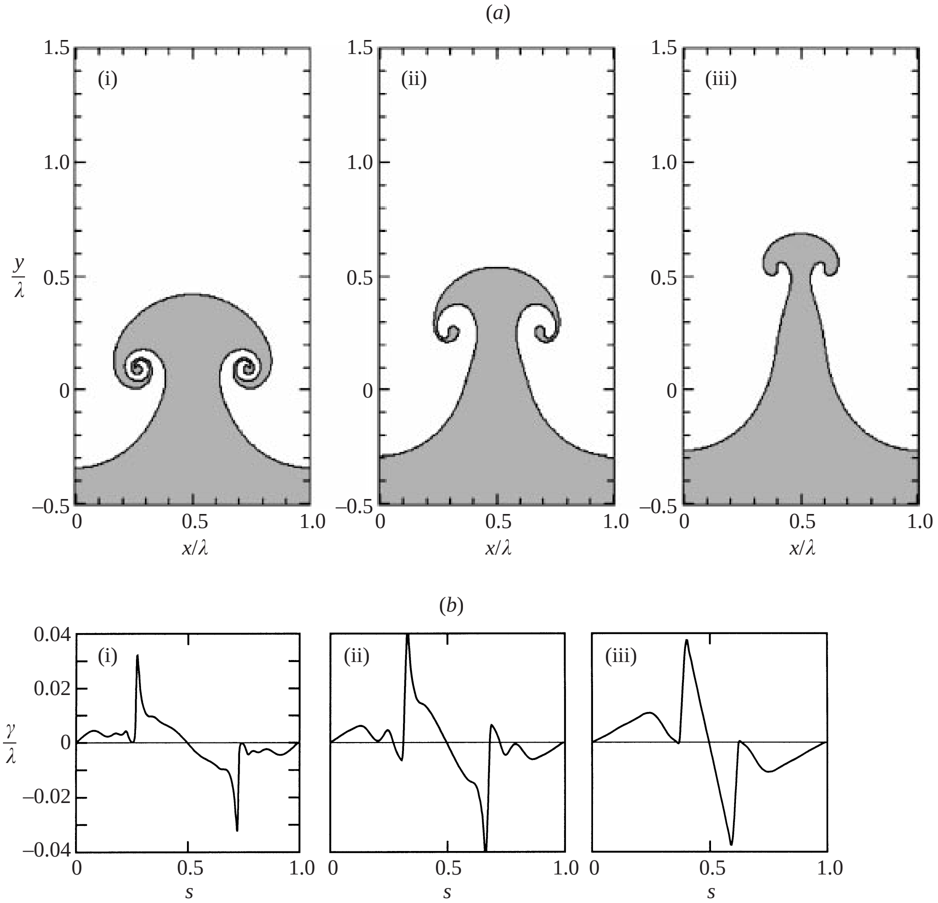

FIGURE 4. (a) Interfaces at Atwood numbers (i) $A = 0.2$, (ii) 0.6 and (iii) 0.9 at time $t = 20$; dimensions of the computational domain are $0 \leqslant x \leqslant \lambda$ and $-2\lambda \leqslant y \leqslant 2\lambda$. ($b$) Circulation per unit length γ_s at the (i) $A = 0.2$, (ii) 0.6 and (iii) 0.9 interfaces at time $t = 20 = 3.2t_M$.

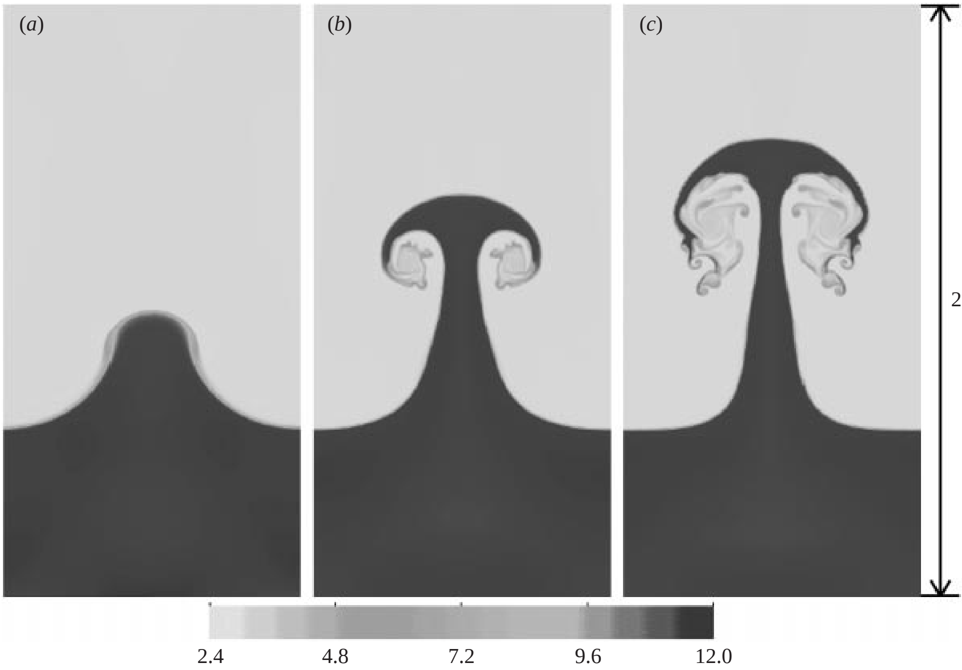

FIGURE 5. The density and vorticity from a PPM simulation of a shock-accelerated interface of air/SF_6 and a finite interfacial transition layer. ($M = 1.55$ and post shock Atwood number of 0.74). Results are shown at times (*a*) t_M, (*b*) $1.63t_M$ and (*c*) $2.63t_M$.

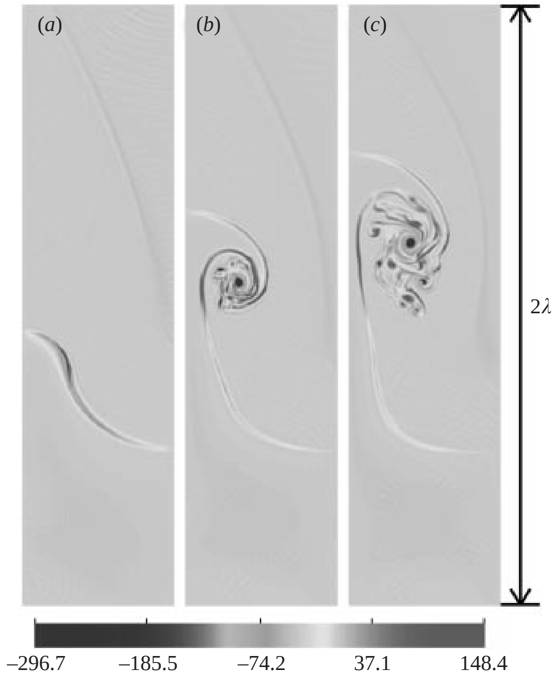

FIGURE 6. Circulations corresponding to the simulation of figure 5.

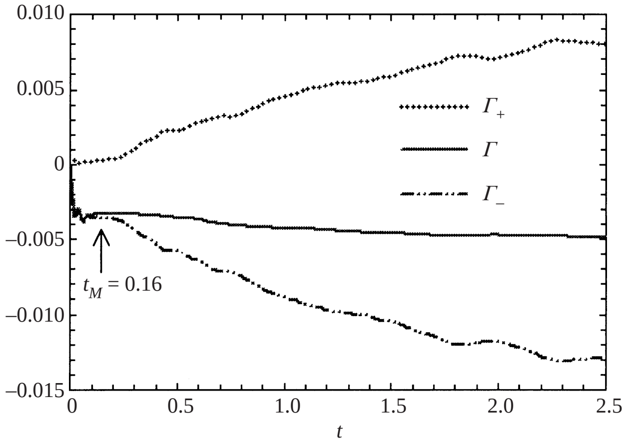

FIGURE 7. Positive, negative and net circulation in the domain between the spike and the bubble extrema. $t_M = 0.16$.

can be fit with the relation

$$\left(\frac{W_m}{\lambda} - \frac{1}{2}\right)/A = -0.33. \tag{10}$$

In figure 4, we compare the evolutions of three A at $t = 20.0$ ($t = 3.2t_M$) with the same initial conditions. The larger A, the larger the amplitude and the smaller the 'roll-up'. That is, baroclinic processes are weaker at low A and do not inhibit roll-up. As A increases, the arc length (s) from the first circulation extrema to the spike is 0.43, 0.33 and 0.19 for $A = 0.2$, 0.6 and 0.9, respectively. Just beyond the extrema nearest to $s = 0.5$, the circulation is nearly discontinuous. These are the locations where the contour changes direction from ingoing to outgoing. For $A = 0.6$ and 0.9, γ/λ changes sign, after the first extremum, a signature that emerges for all cases at later time. This is another manifestation of the baroclinic process, as discussed below.

Note, the minimum width of the neck, W_{min}/λ continues a monotonic decrease after $t_M \approx 6$. We believe that eventually the width goes to zero as the spike region moves away from the bubble region at a nearly constant speed, which depends on the total circulation contained on each side of the axis of symmetry.

2.3. *Numerical results for the interface evolution: compressible*

To validate our incompressible computations and examine results at longer times, we show one well-resolved calculation with the PPM code with a finite interfacial transition layer (ITL) (see Zabusky *et al.* 2002). We resolved the wavelength by 360 zones and used $a_0/\lambda = 0.05$, $\delta_0/a_0 = 0.111$. This choice was made to compare with the incompressible calculations which were made with 128 zones to one wavelength. That is, for the incompressible case, we assumed that the grid-'regularized' ITL was $\frac{1}{16}$ of the wavelength. To correspond to the experiment of Prasad *et al.* (2000), we chose $M = 1.55$ and a post-shock Atwood number of 0.74, corresponding to air/SF$_6$. For simplicity, we use an identical specific heat of $\gamma = 1.4$.

The density and vorticity are shown at three times, t_M, $1.63t_M$ and $2.63t_M$ in figures 5 and 6. Note, the width at t_M agrees with (10). The times in figures 5(b, c) and 6(b, c) are less than the time shown in figure 4(a) for $A = 0.6$ and yet the density plots are more complex in the roll-up region for the compressible finite ITL run.

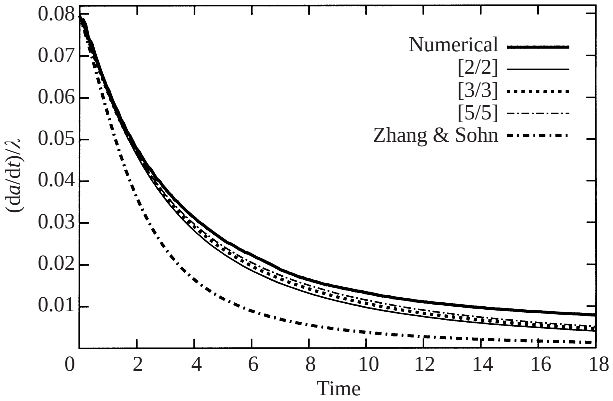

FIGURE 8. Comparison of the normalized interfacial growth rates at Atwood number $A = 0.2$. Shown are the numerical solution and various order $[m/n]$ Padé approximants including Zhang & Sohn (1996). The initial parameters are $a_0 = 0.08\lambda$, $v_0 = 0.08\lambda$.

This arises because the ITL of the compressible run is constantly narrowed (or the density gradient grows) owing to interface stretching. This complexity is also seen in the vorticity and causes the roll-up domain to have different magnitudes, e.g. of minimum neck size or total elongation, than obtained with the incompressible run.

In figure 7, we see that a manifestation of the gradient intensification is the persistent and large growth of positive and negative secondary circulation. This means that the turbulence and mixing properties in the roll-up domain at intermediate and later times will be dependent on the initial conditions. This secondary circulation will be quantified and scaled in a future work. For this case, the growth rate curve in figure 8, can be fitted with $\dot{a} \propto O(t^{-0.68})$, and -0.68 is the filled circle in figure 13.

3. Intermediate and late time comparisons of $\dot{a}$ from numerical and algebraic methods with Padé resummation and with experiment

3.1. *Comparisons of $\dot{a}$: numerical and algebraic methods*

We now compare the amplitude growth rate of (8) from our numerical solutions with our analytical solutions from an eleven-term series, valid for $t < t_M$; and Zhang & Sohn's (1996) four-term series. Since the series solution diverges, we adopt, as Zhang & Sohn did, a Padé rational fraction representation for series. In our notation, $[m/n]$ is indicative of the highest degree polynomial in time, m in the numerator and n in the denominator. Zhang's model was [1/2], so that its long time behaviour was $\dot{a} \approx O(t^{-1})$. In the curves that follow, we present the results of the three best Padé curves out of the many we studied.

In figure 8, we examine the initial conditions $a_0/\lambda = 0.08$, $v_0/\lambda = 0.08$, $(t_N = 1.0)$ for $A = 0.2$. We see that three higher-order Padé approximants, [2/2], [3/3] and [5/5] agree very closely with the numerical result, which is slightly larger than all of them. The Zhang & Sohn [1/2] model begins to depart from this cluster of curves at about $t = 2.0$. In figure 9, for $A = 0.9$, we present comparisons of the numerical results with [3/3], [4/4] and [5/5]. The [4/4] result does best and the others are in as much error as Zhang & Sohn's [1/2], which is lower than all of them. Figures 10 and 11 show

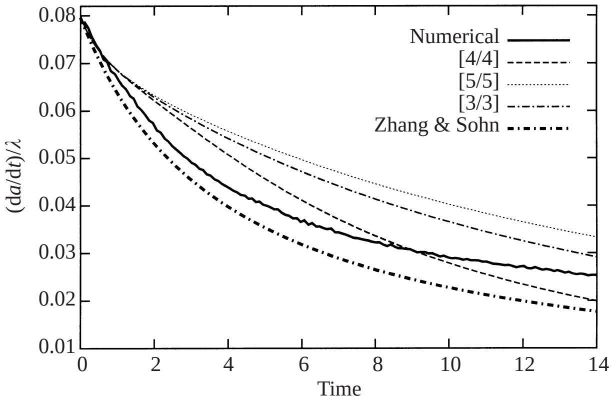

FIGURE 9. Comparison of the normalized interfacial growth rates at Atwood number $A = 0.9$. Shown are the numerical solution and various order $[m/n]$ Padé approximants including Zhang & Sohn (1996). The initial parameters are $a_0 = 0.08\lambda$, $v_0 = 0.08\lambda$.

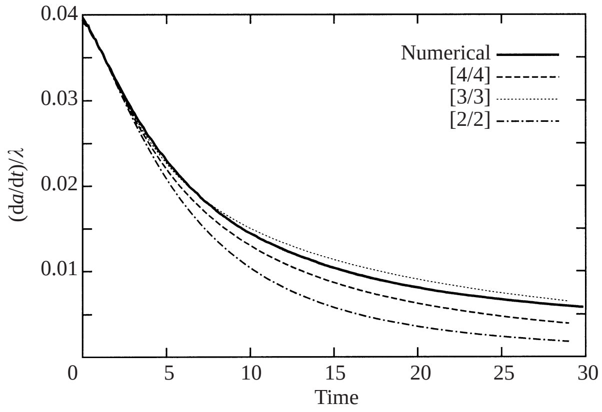

FIGURE 10. Comparison of the normalized interfacial growth rates at Atwood number $A = 0.2$. Shown are the numerical solution and various order $[m/n]$ Padé approximants. The initial parameters are $a_0 = 0.05\lambda$, $v_0 = 0.04\lambda$.

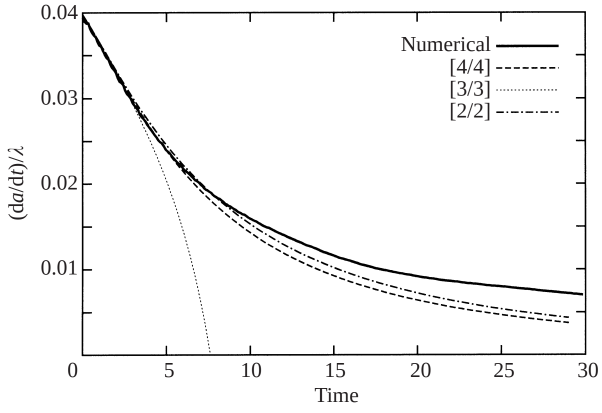

FIGURE 11. Comparison of the normalized interfacial growth rates at Atwood number $A = 0.5$. Shown are the numerical solution and various order $[m/n]$ Padé approximants. The initial parameters are $a_0 = 0.05\lambda$, $v_0 = 0.04\lambda$.

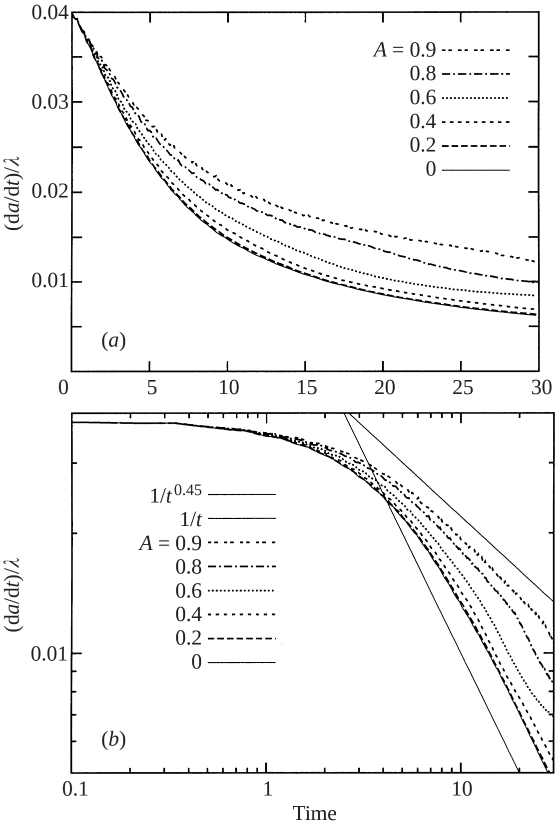

FIGURE 12. Time dependence of the interfacial growth rate $\mathrm{d}a/\mathrm{d}t$ at Atwood numbers $A = 0, 0.2, 0.4, 0.6, 0.8$ and 0.9 at time range $t < 30$. (*a*) Linear axes. (*b*) Logarithmic axes. The two straight lines in (*b*) represent the functions $\dot{a} \propto O(t^{-1.0})$ and $\dot{a} \propto O(t^{-0.45})$ (which approximate, for the intermediate time range, the time dependence of the growth rate at $A = 0$ and $A = 0.9$, respectively).

fits for $A = 0.2$ and 0.5 with, $a_0/\lambda = 0.05$, $v_0/\lambda = 0.04$, $(t_N = 1.25)$. Most fits are very good for $5t < 10$. The [3,3] curve in figure 11 has a zero in the denominator.

We conclude that in most cases the [1,2] Padé representation of Zhang & Sohn is inferior to our higher-order Padé representations. Furthermore, there is not a ‘best’ Padé representation using the 11-term analytical series that we obtained from MuPad.

3.2. *Comparisons of $\dot{a}$: from numerical and experimental methods*

3.2.1. *Incompressible simulations*

In figure 12, we show numerical results for ‘intermediate’ time of $\dot{a}$. It varies from $\dot{a} \propto O(t^{-1})$ for small A to $\dot{a} \propto O(t^{-0.4})$ for $A = 0.9$. The exponents α of fits of (t^{α}) to the intermediate-time numerical data of figure 12 are given in figure 13. Here, we see remarkable agreement with the experiments (Prasad *et al.* 2000) for an $M = 1.55$ shock striking an air/SF_6 interface, which is placed on the graph at 0.68 (filled circle) at $A = 0.74$, the post-shock density ratio. We conclude that during intermediate times, $1 < t/t_M < 3$, the $\dot{a}$ decay exponent, α, varies from −0.4 to −1.0, as A varies from 0.2 to 0.9.

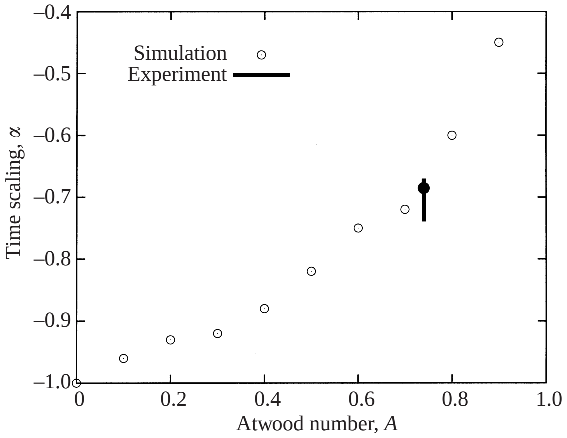

FIGURE 13. Parameter α in the growth rate scaling ($\mathrm{d}a/\mathrm{d}t \sim t^{\alpha}$) *vs.* Atwood number, measured at time $t \sim 20$; the vertical bar represents the experimental results of Prasad *et al.* (2000). The filled circle is from the compressible PPM simulation.

4. Caveats

4.1. *Numerical resolution and non-convergence*

Baker *et al.* (1993) have discussed the generalization of the Moore (1979) singularity to the incompressible Rayleigh–Taylor problem. The manifestation of the ill-posed nature of the problem has also been discussed for compressible simulations by Meiron, Baker & Orszag (1982) and Samtaney & Pullin (1996). In our incompressible CASL/VIC simulations, the interface has at all times an effective finite-layer thickness of about 3–4 cells. This strongly affects the intermediate-time small-scale structures. However, the growth rate, which is the result of averaging vortex effects at two distant points is insensitive to these details, as our finite-ITL PPM simulations show.

4.2. *Power series*

We have used an algebraic series in integer powers of t. However, for problems, as this one, in which singularities arise there may exist ‘exponentially small’ terms which become more important as we approach the singularity time. Furthermore, we believe that the singularity will prevent the continuation of an unregularized series beyond the multivalue time.

5. Summary

In this paper, we have studied, by algebraic and numerical methods, the evolution of a small-amplitude single-mode interfacial perturbation, undergoing RM instability at various Atwood numbers. We identify two temporal stages, ‘early’ and ‘intermediate’, separated by the ‘multivalue’ time.

In the ‘early’ stage, we have improved the analytical theory previously proposed by Zhang & Sohn (1996) and clarified its range of applicability for the growth rate of the interface. We have used the MuPad computer algebra environment, to compute eleven terms in an expansion series in t. The results were compared with vortex-in-cell numerical simulations. It was shown that, at low Atwood numbers, Padé approximants provide a very good agreement with the numerical simulations, even beyond the ‘multivalue’ time. At intermediate Atwood numbers, the agreement is still good before the ‘multivalue’ time, and large discrepancy occurs at late time between the theory and simulations. At high Atwood numbers, we see that the difference between the theory and simulations increases at early times.

At the ‘multivalue’ time, t_M we have shown that the distance between the nearest points, or the spike width, scales linearly with the Atwood number. This phenomenon can be explained by the shift of the maximum circulation per unit length on the interface towards the spike owing to the baroclinic effects. In addition, we have presented the circulation per unit length on the interface, an important small-scale feature to which future studies may be compared.

The growth rate of the interface decreases with time. The higher the Atwood number, the more slowly the growth rate decays. In the intermediate phase, $15 < t < 30$, the growth rate behaves as $\dot{a} \propto O(t^{-1})$ for small A and $\dot{a} \propto O(t^{-0.4})$ for $A = 0.9$. We obtain very good agreement with the experimental results of Prasad *et al.* for incompressible and compressible simulations. However, it remains a challenge to develop accurate initialization procedures and codes to compute the intermediate–late time evolution of the turbulent ‘roll-up’ region.

Beyond intermediate times $t > 3t_M$, we see the strong growth of vortex-accelerated positive and negative circulations in the compressible simulations. In a future work we will quantify, scale and model these results.

This work was supported in part by the Department of Energy (DOE) (Grant DE-FG02-98ER25364, monitored by Dr D. Hitchcock. We appreciate discussions with Professors D. Dritschel (who also gave us his CASL code) and G. Tryggvason, and also with Dr R. Samtaney and Dr J. Ray. Gnuplot (Williams & Kelley 1999) and Yorick (Munro 1994) graphic packages were used in preparation of the manuscript.

Appendix

The literal equations for the Taylor series described in § 2.1 were normalized and the first six are given below. Here we have used

$$\eta^* = \sum_{p=1}^{\infty} \eta^{*(p)}(x,t), \quad \text{where} \quad \eta^{*(p)} = \sum_{j=1}^{j=p} \eta_j^{*(p)}(t)\cos(jkx),$$

where

$$\eta^* = \eta/a_0, \quad \eta_j^{*(p)} = \eta_j^{(p)}/k^{n-1}a_0, \quad \tau = v_0 t/a_0, \quad C_j = \cos(jkx).$$

Note that the first term in the series was obtained by Richtmyer (1960). The second term was given first by Haan (1991) and the third and fourth terms were derived by Zhang & Sohn (1996).

$$\eta_1^* = (1+\tau)C_1,$$

$$\eta_2^* = \tfrac{1}{2}(A\tau^2)C_2,$$

$$\eta_3^* = \tfrac{1}{24}\{-[3\tau^2 + \tau^3 + 4A^2\tau^3]C_1 + 3[-3\tau^2 - \tau^3 + 4A^2\tau^3]C_3\},$$

$$\eta_4^* = \tfrac{1}{12}\{-[3A\tau^2 + 4A^3\tau^4]C_2 + [-A(4\tau^4 + 8\tau^3 - 3\tau^2) + 8A^3\tau^4]C_4\},$$

$$\begin{aligned}\eta_5^* = {} & \left\{ \left[\frac{\tau^2}{12} + \frac{\tau^3}{24} + \frac{1}{192}\tau^4 + \frac{1}{960}\tau^5 \right] + A^2 \left[-\frac{1}{48}\tau^2 + \frac{7}{48}\tau^3 + \frac{11}{48}\tau^4 + \frac{1}{16}\tau^5 \right] + A^4 \left[\frac{1}{60}\tau^5 \right] \right\} C_1 \\ & + \left\{ \left[\frac{3}{128}\tau^5 + \frac{15}{128}\tau^4 + \frac{9}{32}\tau^3 + \frac{7}{32}\tau^2 \right] + A^2 \left[\frac{3}{16}\tau^5 + \frac{1}{4}\tau^4 + \frac{3}{4}\tau^3 \right] - A^4 \left[\frac{27}{40}\tau^5 \right] \right\} C_3 \\ & + \Bigg\{ -\frac{5}{32}\tau^2 + \frac{5}{32}\tau^3 + \frac{35}{128}\tau^4 + \frac{7}{128}\tau^5 \Bigg] + A^2 \left[\frac{5}{8}\tau^3 - \frac{5}{4}\tau^4 - \frac{37}{48}\tau^5 \right] + A^4 \left[\frac{25}{24}\tau^5 \right] \Bigg\} C_5,\end{aligned}$$

$$\begin{aligned}\eta_6^* = {} & \Bigg\{ A \left[\frac{35}{192}\tau^2 - \frac{1}{8}\tau^3 + \frac{13}{96}\tau^4 - \frac{13}{120}\tau^5 - \frac{17}{720}\tau^6 \right] \\ & + A^3 \left[\frac{15}{32}\tau^4 + \frac{19}{40}\tau^5 + \frac{1}{8}\tau^6 \right] + A^5 \left[\frac{1}{10}\tau^6 \right] \Bigg\} C_2 \\ & + A \left[-\frac{7}{32}\tau^2 + \frac{29}{36}\tau^3 + \frac{7}{8}\tau^4 + \frac{2}{15}\tau^5 + \frac{11}{360}\tau^6 \right] \\ & + A^3 \left[-\frac{23}{12}\tau^4 + \frac{9}{10}\tau^5 + \frac{277}{360}\tau^6 \right] - A^5 \left[\frac{64}{45}\tau^6 \right] \Bigg\} C_4 \\ & + \left\{ A \left[\frac{3}{32}\tau^2 - \frac{3}{4}\tau^3 + \frac{1}{4}\tau^4 + \frac{23}{20}\tau^5 + \frac{23}{80}\tau^6 \right] + A^3 \left[\frac{23}{16}\tau^4 - \frac{5}{2}\tau^5 - \frac{7}{4}\tau^6 \right] + A^5 \left[\frac{9}{5}\tau^6 \right] \right\} C_6.\end{aligned}$$

The terms for $p = 7$ to 9 are very lengthy and can be obtained from the authors or the *Journal of Fluid Mechanics* Editorial Office, Cambridge.

REFERENCES

Aleshin, A. N., Azareva, E. V., Chebotareva, E. I., Sergeev, S. V. & Zaytsev, S. G. 1997 Investigation of Richtmyer–Meshkov instability by the incident and the reflected shock waves. In *Proc. 6th Intl Workshop on the Physics of Compressible Turbulent Mixing, Marseille, France, 18–21 June*, pp. 1–5.

Andronov, V. A., Bakhrakh, S. M., Meshkov, E. E., Mokhov, V. N., Nikiforov, V. V., Pevnizhitskii, A. V. & Tolshmyakov, T. 1972 Turbulent mixing on the interface accelerated by shock waves. *Sov. Phys., J. Exp. Theor. Phys.* **71**, 806.

Baker, G., Càflisch, D. R. & Siegel, M. 1993 Singularity formation during the Rayleigh–Taylor instability. *J. Fluid Mech.* **252**, 51–78.

Dimonte, G. & Remington, B. 1993 Richtmyer–Meskov experiment on the nova laser at high compression. *Phys. Rev. Lett.* **70**, 1806–1809.

Dritschel, D. G. & Ambaum, M. H. P. 1997 A contour-advective semi-Lagrangian numerical algorithm for simulating fine-scale conservative dynamical fields. *Q. J. R. Met. Soc.* **123**, 1097.

Grove, J. W. 1994 Applications of front tracking to the simulations of shock refractions and unstable mixing. *J. Appl. Num. Maths* **14**, 213–237.

Gupta, S. & Zabusky, N. J. 2002 Shock gaseous cylinder interactions: secondary baroclinic circulation generation, instability and vortex projectiles. *Phys. Fluids*, submitted.

Haan, S. W. 1991 Weekly nonlinear hydrodynamic instabilities in inertial fusion. *Phys. Fluids* B **3**, 2349–2355.

Hawley, J. F. & Zabusky, N. J. 1989 Vortex paradigm for shock accelerated density stratified interfaces. *Phys. Rev. Lett.* **63**, 1241–1244.

Hecht, J., Alon, U. & Shvarts, D. 1994 Potential flow models of Rayleigh–Taylor and Richtmyer–Meshkov bubble fronts. *Phys. Fluids* **6**, 4019–4030.

Jacobs, J. W., Jenkins, D. G., Klein, D. L. & Benjamin, R. F. 1995 Nonlinear growth of the shock-accelerated instability of a thin fluid layer. *J. Fluid Mech.* **295**, 23–42.

Kotelnikov, A. D. & Montogomery, D. C. 1997 A kinetic method for computing inhomogenous fluid behavior. *J. Comput. Phys.* **134**, 364–388.

Kotelnikov, A. D. & Montogomery, D. C. 1998 Shock induced turbulence at moderate Reynolds numbers. *Phys. Fluids* **10**, 2037–2054.

Kotelnikov, A., Ray, J. & Zabusky, N. 2000 Vortex morphologies on reaccelerated interfaces: visualization, quantification and modeling of one-and-two mode compressible and incompressible environments. *Phys. Fluids* **12**, 3245–3264.

Layzeb, D. 1955 On the gravitational instability of two superposed fluids in a gravitational field. *Astrophys. J.* **122**, 1–12.

Meiron, D. I., Baker, G. R. & Orszag, S. A. 1982 Analytic structure of vortex sheet dynamics. Part 1. Kelvin–Helmholtz instability. *J. Fluid Mech.* **114**, 283–298.

Meiron, D. & Meloon, M. 1997 Richtmyer–Meshkov instability in compressible stratified fluids. In *Proc. 6th Intl Workshop on the Physics of Compressible Turbulent Mixing, Marseille, France, 18–21 June*, pp. 337–342.

Meshkov, E. E. 1969 Interface of two gases accelerated by a shock wave. *Fluid Dyn.* **4**, 101–104.

Meyer, K. A. & Blewett, P. J. 1972 Numerical investigation of the stability of a shock-accelerated interface between two fluids. *Phys. Fluids* **15**, 753–759.

Mikaelian, K. O. 1993 Growth rate of the Richtmyer–Meshkov instability at shocked interfaces. *Phys. Rev. Lett.* **71**, 2903–2906.

Moore, D. W. 1979 The spontaneous appearance of singularity in the shape of an evolving vortex sheet. *Proc. R. Soc. Lond.* A **365**, 105.

Munro, D. H. 1994 *Yoric: An Interpreted Language*. University of California, Lawrence Livermore National Laboratory, ftp://ftp-icf.llnl.gov/pub/Yorick/ydoc/hand/Top.html.

MuPAD Group. 1996 *MuPAD User's Manual – MuPAD Version 1.2.2*. John Wiley: 0-471-96716-5; Teubner: 3-519-02114-5.

Pham, T. & Meiron, D. I. 1993 A numerical study of Richtmyer–Meshkov instability in continuously stratified fluids. *Phys. Fluids* A **5**, 344–368.

Picone, J. M. & Boris, J. P. 1988 Vorticity generation by shock propagation through bubbles in a gas. *J. Fluid Mech.* **189**, 23–51.

Prasad, J. K., Rasheed, A., Kumar, S. & Sturtevant, B. 2000 The late-time development of the Richtmyer–Meshkov instability. *Phys. Fluids* **12**, 2108–2115.

Ray, J. 1999 Shock interaction with density inhomogeneities: models and scaling laws for circulation deposition and instability growth rates. PhD thesis, Rutgers University.

Richtmyer, R. D. 1960 Taylor instability in schock acceleration of compressible fluids. *Commun. Pure Appl. Maths* **13**, 297–319.

Samtaney, R. & Pullin, D. I. 1996 On initial-value and self-similar solutions of the compressible Euler equations. *Phys. Fluids* **8**, 2650–2655.

Samtaney, R. & Zabusky, N. J. 1994 Circulation deposition on shock-accelerated planar and density-stratified interfaces: models and scaling laws. *J. Fluid Mech.* **269**, 45–78.

Tryggvason, G. 1988 Numerical simulations of the Rayleigh–Taylor instabilities. *J. Comput. Phys.* **75**, 253–282.

Velikovich, A. & Dimonte, G. 1996 Nonlinear perturbation theory of the incompressible Richtmyer–Meshkov instability. *Phys. Rev. Lett.* **76**, 3112–3115.

Williams, T. & Kelley, C. 1999 Gnuplot: An Interactive Plotting Program. http://www.gnuplot.vt.edu.

Wouchuk, J. C. & Nishihara, K. 1996 Linear perturbation growth at a shocked interface. *Phys. Plasmas* **3**, 3761–3776.

Wouchuk, J. C. & Nishihara, K. 1997 Asymptotic growth in the linear Richtmyer–Meshkov instability. *Phys. Plasmas* **4**, 1028–1038.

Yang, Y., Zhang, Q. & Sharp, D. 1994 Small amplitude theory of Richtmyer–Meshkov instability. *Phys. Fluids* **6**, 1856–1873.

Youngs, D. L. 1984 Numerical simulation of turbulent mixing by Rayleigh–Taylor instability. *Physica* D **2**, 32–44.

Zabusky, N. J. 1999 Vortex paradigm for accelerated inhomogeneous flows: visiometrics for the Rayleigh–Taylor and Richtmyer–Meshkov environments. *Annu. Rev. Fluid Mech.* **31**, 495–535.

Zabusky, N. J., Gupta, S., Samtaney, R. & Gulak, J. Y. 2002 Localization and spreading of contact discontinuity layers in simulations of compressible dissipationless flows. *Comput. Phys.*

Zaytsev, S. G., Lazareva, E. V., Chernukha, V. V. & Belyaev, V. M. 1985 Intensification of mixing on the interface between different density media at shock passage. *Dokl. Akad. Nauk SSSR* **283**, 94–98.

Zhang, Q. & Sohn, S. 1996 Nonlinear theory of unstable fluid mixing driven by shock wave. *Phys. Fluids* **9**, 1106–1124.